



HAL
open science

Analysis of nucleic acid chaperoning by the prion protein and its inhibition by oligonucleotides

Cécile Guichard, Roland Ivanyi-Nagy, Kamal Kant Sharma, Caroline Gabus, Daniel Marc, Yves Mély, Jean-Luc Darlix

► **To cite this version:**

Cécile Guichard, Roland Ivanyi-Nagy, Kamal Kant Sharma, Caroline Gabus, Daniel Marc, et al.. Analysis of nucleic acid chaperoning by the prion protein and its inhibition by oligonucleotides. *Nucleic Acids Research*, 2011, 39 (19), pp.8544-8558. 10.1093/nar/gkr554 . hal-02645493

HAL Id: hal-02645493

<https://hal.inrae.fr/hal-02645493>

Submitted on 29 May 2020

HAL is a multi-disciplinary open access archive for the deposit and dissemination of scientific research documents, whether they are published or not. The documents may come from teaching and research institutions in France or abroad, or from public or private research centers.

L'archive ouverte pluridisciplinaire **HAL**, est destinée au dépôt et à la diffusion de documents scientifiques de niveau recherche, publiés ou non, émanant des établissements d'enseignement et de recherche français ou étrangers, des laboratoires publics ou privés.



Distributed under a Creative Commons Attribution - NonCommercial 4.0 International License

Analysis of nucleic acid chaperoning by the prion protein and its inhibition by oligonucleotides

Cécile Guichard¹, Roland Ivanyi-Nagy¹, Kamal Kant Sharma², Caroline Gabus¹, Daniel Marc³, Yves Mély² and Jean-Luc Darlix^{1,*}

¹Unité de Virologie Humaine INSERM, ENS, IFR 128, 46 allée d'Italie, 69364 Lyon, ²UMR 7213 CNRS, Laboratoire de Biophotonique et Pharmacologie, Faculté de Pharmacie, Université de Strasbourg, 74 route du Rhin, 67401 Illkirch and ³INRA, Nouzilly, TOURS, France

Received April 12, 2011; Revised June 11, 2011; Accepted June 16, 2011

ABSTRACT

Prion diseases are unique neurodegenerative illnesses associated with the conversion of the cellular prion protein (PrP^C) into the aggregated misfolded scrapie isoform, named PrP^{Sc}. Recent studies on the physiological role of PrP^C revealed that this protein has probably multiple functions, notably in cell–cell adhesion and signal transduction, and in assisting nucleic acid folding. In fact, *in vitro* findings indicated that the human PrP (huPrP) possesses nucleic acid binding and annealing activities, similarly to nucleic acid chaperone proteins that play essential roles in cellular DNA and RNA metabolism. Here, we show that a peptide, representing the N-terminal domain of huPrP, facilitates nucleic acid annealing by two parallel pathways nucleated through the stem termini. We also show that PrP of human or ovine origin facilitates DNA strand exchange, ribozyme-directed cleavage of an RNA template and RNA *trans*-splicing in a manner similar to the nucleocapsid protein of HIV-1. In an attempt to characterize inhibitors of PrP-chaperoning *in vitro* we discovered that the thioaptamer 5'-GACACAAGC CGA-3' was extensively inhibiting the PrP chaperoning activities. At the same time a recently characterized methylated oligoribonucleotide inhibiting the chaperoning activity of the HIV-1 nucleocapsid protein was poorly impairing the PrP chaperoning activities.

INTRODUCTION

Transmissible spongiform encephalopathies (TSEs) such as Creutzfeldt-Jakob disease (CJD), kuru and fatal

familial insomnia (FFI) in humans, scrapie in sheep and bovine spongiform encephalopathy (BSE) in cattle are a group of fatal neurodegenerative diseases (1–3). A major molecular characteristic of TSEs is the accumulation of a misfolded, aggregated, partially protease-resistant prion protein (PrP), named PrPres, in the central nervous system (CNS) (1–3). Accumulation of PrPres appears to take place by recruitment and templated transconformation of the normal cellular prion protein (PrP^C) by PrPres (4–7), and is thought to induce functional damages to the CNS. In support of this, generation of spongiform encephalopathy requires the presence of both PrPres and PrP^C since mice devoid of PrP^C are resistant to challenge with the infectious prion agent (8).

The PrP^C is highly conserved in mammals and abundantly expressed in cells of the nervous and lymphoreticular systems but its physiological role has remained for a long time a matter of speculation (2,9). In fact, PrP null mice were found to develop and reproduce normally (10), or manifested only subtle phenotypic effects [reviewed in (11)], suggesting that PrP^C has no essential function(s) that could not be compensated by proteins with overlapping activities. Nevertheless, several functions have been proposed for PrP^C, including superoxide dismutase activity (12,13), participation in copper metabolism (14), signal transduction (15) and neuroprotection [(16,17), and references therein]. Recent studies revealed that PrP^C has a crucial role in cell–cell adhesion and in signal transduction mediated by Src-related kinases in the zebrafish animal model (18). In addition, there are clear indications that PrP^C assists nucleic acid folding and interactions in a manner similar to cellular and viral nucleic acid chaperones *in vitro* (19–21), and might well restrict retrovirus replication (22,23).

In fact, there are many different nucleic acid binding proteins that recognize DNA and RNA with a broad

*To whom correspondence should be addressed. Tel: +33472728169; Fax: +33472728137; Email: jldarlix@ens-lyon.fr

Present address:

Roland Ivanyi-Nagy, Molecular Parasitology Group, The Weatherall Institute of Molecular Medicine, University of Oxford, Oxford, OX3 9DS, UK.

The authors wish it to be known that, in their opinion, the first two authors should be regarded as joint First Authors.

© The Author(s) 2011. Published by Oxford University Press.

This is an Open Access article distributed under the terms of the Creative Commons Attribution Non-Commercial License (<http://creativecommons.org/licenses/by-nc/3.0>), which permits unrestricted non-commercial use, distribution, and reproduction in any medium, provided the original work is properly cited.

sequence specificity in any given cell. Among these ubiquitous nucleic acid binding proteins (NABP) there exists a class named nucleic acid chaperones, which provide assistance to the folding of DNA and RNA by preventing and resolving misfolding, and by chaperoning DNA/RNA interactions (24,25). Thus nucleic acid chaperones are considered to be essential co-factors for many basic biological processes including nucleic acid maintenance, RNA splicing, transport and translation (24,25) and PrP^C would be one of these proteins (19–21).

In an attempt to better understand the relationship between the PrP^C and nucleic acids and its possible role in nucleic acid metabolism, we investigated the nucleic acid chaperoning activities of the recombinant human and ovine PrP *in vitro*. Using fluorescence resonance energy transfer (FRET), we report that a prion peptide representing the N-terminal domain of huPrP is very active in facilitating nucleic acid annealing. Furthermore, by using established nucleic acid chaperoning assays, notably DNA strand transfer (26), ribozyme cleavage of an RNA substrate (27,28) and RNA *trans*-splicing (29,30), we show that the human and ovine PrPs are potent nucleic acid chaperones. Recently we have been able to characterize a potent oligonucleotide (ODN) inhibitor of the nucleic acid chaperoning activity of the HIV-1 nucleocapsid protein (NC) *in vitro* and its inhibitory effect on virus replication in primary human cells (31). This prompted us to search for ODNs capable of inhibiting the nucleic acid chaperoning activity of PrP. We discovered that a previously identified 5'-GACACAAGCCGA-3' thioaptamer binding to Syrian hamster (SHa) and human PrP (32) was a potent inhibitor of PrP-chaperoning activity *in vitro*, while the non-modified ODN was not, and a methylated ODN specific for HIV-1 NC was slightly inhibitory.

MATERIALS AND METHODS

Recombinant proteins

Recombinant human PrP (huPrP from residues 23–231), the N-terminal region [huPrP(23–145)] and the C-terminal region [huPrP(122–231)] were expressed in *Escherichia coli* and purified to homogeneity (19). The N-terminal region 23–110 of huPrP was synthesized by fmoc chemistry and purified to homogeneity by HPLC (19). The ovine PrP (ovPrP, residues 25–234) was produced in *E. coli* and purified to homogeneity (33). HIV-1 nucleocapsid protein NCp7 and NC(12–53) lacking the N- and C-terminal regions were obtained as pure proteins as previously described (19,34). Proteins were dissolved at 1 mg/ml in buffer containing 30 mM HEPES pH 6.5, 30 mM NaCl and 0.1 mM ZnCl₂. HnRNP A1 and YB-1/p50 were provided by Christiane Branlant (France) and Lev Ovchinnikov (Russia), respectively.

Plasmid DNAs and RNAs

Plasmids pS14, pS20 and pR3, for the ribozyme assays, were provided by E. Bertrand (Montpellier) (28) and plasmids H1 and H2 for the *trans*-splicing assays by Renée Schroeder (Vienna, Austria). All plasmid DNAs

were amplified in *E. coli* Rec A- cells and purified by affinity chromatography (Qiagen, USA). H1 DNA (549 nt of exon 1 and 131 nt of the 5' part of the intron) was linearized with Sall and H2 DNA (147 nt of the 3' half of the intron and 23 nt of exon 2) was linearized with BamHI, then transcribed. Templates pS14, pS20 and pR3 were digested by Pst I, treated by Klenow polymerase to remove the 3' strand overhang, and then the substrate RNA and the ribozyme were generated by *in vitro* transcription with modifications: for substrate RNA UTP was at 10 μM and 50 μCi ³²P-UTP (Amersham, UK) was added. For the ribozyme, UTP was at 100 μM with 10 μCi of ³²P-UTP. For the *trans*-splicing assays, RNAs H1 and H2 were prepared by *in vitro* transcription with T7 RNA polymerase according to the manufacturer's instructions (Promega) and labelled by incorporation of ³⁵S-UMP during transcription.

Following RNA synthesis, the DNA template was removed by treatment with RNase-free DNase I (Promega) for 20 min at 37°C, followed by phenol extraction and ethanol precipitation. All RNAs were purified by 8% PAGE in 7M urea, 0.5× TBE. RNAs were recovered by elution in 0.3M sodium acetate, 0.1% SDS, for 4 h at 37°C and ethanol precipitated. RNAs were dissolved in sterile H₂O and their integrity was verified by PAGE-urea.

TAR DNA

ODNs used for DNA annealing corresponded to the HIV-1 TAR sequences, in the sense and antisense orientations, respectively. ODNs were purchased from Eurogentec (Belgium). TAR ODNs are 56 nt in length.

TAR(+) (sense):

5'-GGTCTCTCTTGTTAGACCAGGTCGAGCCCCG
GGAGCTCTCTGGCTAGCAAGGAACCC-3';

TAR(-) (antisense):

5'-GGGTTCCCTTGCTAGCCAGAGAGCTCCCGGG
CTCGACCTGGTCTAACAAGAGAGACC-3';

ODNs used for DNA strand transfer assays corresponded to the HIV-1 repeated R sequences, in the sense and antisense orientations, already described in (35,36).

TAR(-) and R(+) ODN were ³²P-labelled with 50 μCi of ³²P-ATP using T4 polynucleotide kinase. Labelled ODNs were purified by 10% PAGE, 7M urea in 50 mM Tris-borate, 1 mM EDTA, pH 8.3 (0.5× TBE) and recovered, ethanol precipitated and dissolved in sterile H₂O before use.

Oligonucleotides

The 12-nt long thioaptamer (GA-12; 5'-GACACAAGCCGA-3'), with five modifications 5' to the dA residues, mODN-11 (5'-GGUUUUUGUGU-3' with a 2'-O-methyl modification at each residue) and ODN-11 (5'-GGTTTTTGTGT-3', without modifications) were obtained in a highly pure form from Eurogentec (Belgium). Ct-12 corresponds to GA-12 without the modifications.

Destabilization assay

To monitor the nucleic acid destabilizing properties of huPrP, cTAR DNA was labelled either by carboxytetramethylrhodamine (TMR) or ethyl 2-[3-(ethylamino)-6-ethyl-imino-2,7-dimethylxanthen-9-yl]benzoate hydrochloride (Rh6G) at its 5'-end, while the 3' terminus was labelled with either 4-(4'-dimethylaminophenylazo) benzoic acid (Dabcyl) or 5-(and 6)-carboxyfluorescein (Fl). The dyes form a non-fluorescent heterodimer when the cTAR stem is closed, while melting of the stem restores the fluorophore fluorescence. Thus, the destabilizing ability of HuPrP peptide (23–110) was evaluated from the ratio of the fluorescence intensity in the presence versus the absence of the peptide. Experiments were performed by adding huPrP (23–110) at increasing peptide to oligonucleotide ratio to 50 nM doubly labelled cTAR, in 25 mM Tris, 30 mM NaCl and 0.2 mM MgCl₂, pH 7.5.

Kinetics of cTAR-dTAR annealing with the huPrP peptide (23–110)

The real-time annealing kinetics of cTAR with dTAR was investigated by mixing Rh6G-5'-cTAR-3'-Dabcyl with an excess of non-labelled dTAR in conditions already published (35,37). Formation of the 55-bp cTAR/dTAR extended duplex (ED) strongly increases the interchromophore distance, leading to a full recovery of Rh6G emission. The dependence of cTAR-dTAR annealing kinetics on temperature was performed at six different temperatures, viz. 15, 20, 25, 30, 35 and 40°C, as previously described (37).

The TAR(-)/TAR(+) annealing assay

Tar(+) and ³²P-Tar(-) ODNs were incubated (0.03 pmol each) in 10 µl of buffer A (35,37) in the presence of increasing protein concentrations. Reactions were performed at 37°C for 5 min except for the positive control which was incubated at 65°C. To stop the reaction and denature the protein, we added 5 µl of a solution containing 20% glycerol, 20 mM EDTA, pH 8.0, 2% SDS, 0.25% bromophenol blue and 0.4 mg/ml calf-liver tRNA. Samples were resolved by 8% native PAGE in 50 mM Tris-Borate, pH 8.3, 1 mM EDTA at 4°C. Subsequently, gels were autoradiographed and the amounts of labelled single-stranded and double-stranded DNA were assessed by PhosphorImaging.

Effect of inhibitors on the kinetics of cTAR-dTAR annealing with the N-terminal huPrP

Inhibition of huPrP(23–110)-promoted cTAR-dTAR annealing was performed by adding a 5-fold molar excess of GA-12, mODN-11 or Ct-12 relative to cTAR/dTAR. The cTAR (or dTAR)-huPrP(23–110)-ODN mixtures were incubated for 5 min to ensure that the binding equilibrium was reached. Then, cTAR-dTAR hybridization was initiated by manual mixing of cTAR-huPrP (23–110)-ODN mixture with dTAR-huPrP(23–110)-ODN mixture. To avoid the effects of local concentration fluctuations on the annealing kinetics, equal volumes of the mixtures were used. Experiments were performed in

pseudo-first order conditions by mixing 10 nM of doubly labelled cTAR with 300 nM of non-labelled dTAR in presence of huPrP(23–110) at a peptide/oligonucleotide molar ratio of 1:1. To this mixture, inhibitors were added in increasing concentrations (from 0.1- to 10-fold) to follow their concentration dependent inhibitory effect.

All experiments were performed in 25 mM Tris-HCl (pH 7.5), 30 mM NaCl, 0.2 mM MgCl₂ at 20°C.

DNA strand transfer assay

³²P-labelled R(+) wt, non-labelled R(-) 3'-modified and R(-) wt were heat denaturated (2 min at 90°C) and chilled on ice. All components were kept on ice. An amount of 0.03 pmol each of R(+) wt and R(-) 3'-modified were mixed with reaction buffer to a final concentration of 20 mM Tris-HCl, pH 7.0, 30 mM NaCl, 0.1 mM MgCl₂, 10 µM ZnCl₂ and 5 mM DTT in 5 µl final volume, incubated for 30 min at 65°C and chilled on ice. Subsequently, 0.03 pmol R(-) wt was added together with the chaperone protein at a final protein to nucleotide molar ratio as indicated in figure legends. Reactions were left to proceed for 1–5 min at 37°C. The mixtures were then chilled on ice and reactions stopped with 2.5 µl of 20% glycerol, 20 mM EDTA pH 8.0, 0.2% SDS, 0.25% bromophenol blue and 0.4 mg/ml calf liver tRNA. Samples were resolved by 6% native PAGE in 50 mM TBE at 4°C. The level of strand exchange as a function of time was quantified by PhosphorImaging.

Hammerhead Ribozyme cleavage assay

Ribozyme and substrate RNAs were independently heated for 1 min at 90°C in H₂O. The reaction buffer was added to yield final concentrations of 5 mM MgCl₂, 100 mM NaCl, 20 mM Tris-HCl, pH 7.5. After slowly cooling down to 37°C, RNAs were further incubated for 5 min at 20°C. An amount of 0.1 pmol of ribozyme and 0.02–2 pmol of RNA substrate were then combined in a final volume of 10 µl, each protein was added at final concentrations as indicated in the figure legend and incubations were for 1–30 min at 37°C. Reactions were terminated by adding 20 µl of stop solution (0.3% SDS, 15 mM EDTA), and RNAs were extracted with 30 µl of phenol and 15 µl of chloroform. The aqueous phase was precipitated with ethanol and the pellet resuspended in 45% formamide, 0.5× TBE, and 0.1% dye. RNAs were then analysed on 8% PAGE in TBE. All quantitative measurements were done by PhosphorImaging.

Trans-splicing assay

An amount of 2×10^{-8} M each of ³⁵S-labelled RNAs were incubated for 1 min at 95°C in H₂O and cooled down to 37°C. Then, the splicing buffer (40 mM Tris-Cl at pH 7.4, 3 mM MgCl₂, 0.4 mM spermidine, 4 mM DTT), 8 U RNasin (Promega) and ³²P-GTP were added with the nucleic acid chaperone, at protein to nucleotide molar ratios as indicated in the figure legend, at 37°C for 30 min in 10 µl. Reactions were stopped by adding a final concentration of 40 mM EDTA and 300 µg/ml of tRNA. Proteins were removed by phenol-chloroform

extraction, and nucleic acids precipitated by ethanol. Samples were resuspended in 10 μ l formamide buffer (97% formamide, 1 mM EDTA, 0.02% bromophenol blue, 0.02% xylene cyanol), denatured for 2 min at 95°C and resolved by denaturing 5% PAGE-7M Urea in 0.5 \times TBE. Subsequently, the gel was fixed, dried and autoradiographed. 5' 32 P-labelled FX174 DNA *Hinf*I markers (Promega) were used for size determination (data not shown). Bands corresponding to the product of the first step of splicing (corresponding to the G-II RNA, 132 nt in length) were measured by PhosphorImager.

RESULTS

In order to examine the nucleic acid chaperoning (24,25,38) properties of the PrP, we have used advanced assays [reviewed in (39)] that have been developed for the characterization of key chaperone proteins implicated in the metabolism of cellular RNAs such as hnRNP A1 and FMRP proteins (28,40–42), and of retroviral RNA, like the NC protein of retroviruses [(26,28,42), reviewed in (43,44)]. Although the details of their mechanism of action is incompletely understood, nucleic acid chaperones are thought to facilitate RNA (and DNA) conformational rearrangements by a variety of ATP-independent mechanisms, including destabilization of preformed helices, charge neutralization and matchmaker activity (24,25,45,46).

First, we have analysed the helix destabilizing activity of the N-terminal peptide (23–110) of huPrP. Using the doubly labelled cTAR DNA stem-loop (SL), there was no evidence of helix destabilizing activity of huPrP(23–110) in the present conditions, as observed by FRET (Figure 1A and Supplementary Data). This differs from HIV-1 NC protein, which shows significant helix destabilizing activity (47–49) (data not shown), but is similar to the behaviour of the core protein of hepatitis C virus (HCV), another well-characterized RNA chaperone with limited cTAR melting activity (37). Next, we monitored the impact of huPrP(23–110) on the annealing kinetics of cTAR/dTAR by FRET.

Kinetics of cTAR-dTAR annealing facilitated by the N-terminal peptide of huPrP

The real-time annealing kinetics of cTAR to dTAR was investigated in pseudo-first order conditions by mixing Rh6G-5'-cTAR-3'-Dabcyl with an excess of non-labelled dTAR (35,37). Formation of the 55-bp cTAR/dTAR ED strongly increases the interchromophore distance, leading to a full recovery of Rh6G emission. In the absence of huPrP(23–110), the annealing of cTAR with dTAR was very slow, involving two distinct kinetic components with second-order rate constants. In the presence of huPrP(23–110) at a peptide/TAR ratio of 1/1, the same fluorescence plateau was observed as in the absence of peptide, indicating that ED formation went to completion. The huPrP(23–110) strongly accelerated the annealing reaction, since it was completed in \sim 30 min, instead of >1 day without the peptide. An adequate fit

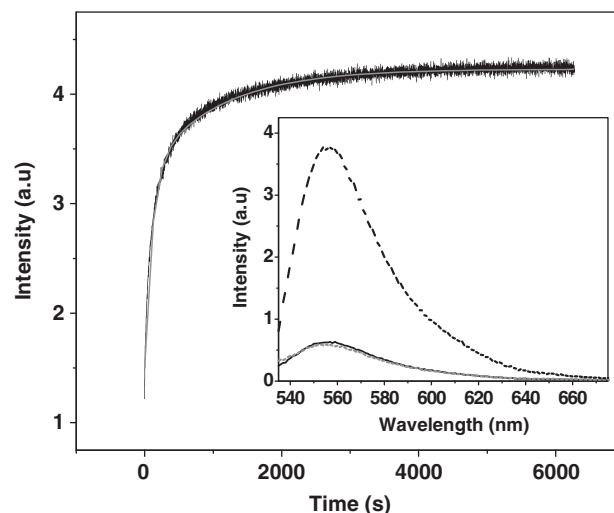


Figure 1. Promotion of cTAR/dTAR annealing by huPrP(23–110). Kinetic trace of 10 nM Rh6G-5'-cTAR-3'-Dabcyl with 100 nM of dTAR in 25 mM Tris-HCl (pH 7.5), 30 mM NaCl, 0.2 mM MgCl₂ at 20°C. huPrP(23–110) was added at a 1:1 molar ratio to cTAR and dTAR. Excitation and emission wavelengths were 520 nm and 550 nm, respectively. The continuous grey line corresponds to the best fit of the data according to Equation (1), using $k_{\text{obs1}} = 5.6 \times 10^{-3} \text{ s}^{-1}$, $k_{\text{obs2}} = 6.8 \times 10^{-4} \text{ s}^{-1}$ and $a = 0.7$. Inset: Emission spectra of 10 nM doubly labelled cTAR (solid line), with 10 nM huPrP(23–110) (dotted line) and with 100 nM dTAR + 100 nM huPrP(23–110) after completion of the annealing reaction (dashed line).

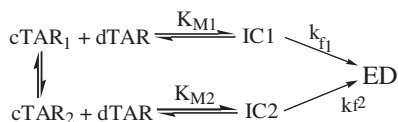
of the annealing kinetic traces was obtained using a bi-exponential function:

$$I(t) = I_f - (I_f - I_0) \left(a e^{-k_{\text{obs1}}(t-t_0)} - (1-a) e^{-k_{\text{obs2}}(t-t_0)} \right) \quad (1)$$

where t_0 is the dead time, $k_{\text{obs1,2}}$ are the observed kinetic rate constants, a is the amplitude of the fast component, and I_0 and I_f are the fluorescence intensities of the SL and the ED, respectively.

We already observed a fast and full fluorescence increase at the lowest tested oligonucleotide concentrations (10 nM cTAR and 100 nM dTAR) (Figure 1), suggesting that the peptide probably binds to the TAR sequences with a high affinity ($>10^7 \text{ M}^{-1}$). Indeed, if the binding constant would be $<10^6 \text{ M}^{-1}$, and if we assume that, as for other nucleic acid chaperones, PrP does not exhibit any catalytic activity, most of the oligonucleotides would be free and would anneal at the low speed observed for cTAR and dTAR in the absence of protein.

Annealing as a function of the dTAR concentration indicated a saturation behaviour of both k_{obs1} and k_{obs2} values as well as a constant value for their amplitudes (Supplementary Figure S1B and Supplementary Data). Moreover, the values of the intercept for both k_{obs1} and k_{obs2} curves were very low, indicating that huPrP(23–110) is unable to dissociate the ED. Based on these kinetic data, a reaction mechanism with two parallel pathways can be proposed (scheme 1), as for the HCV core-promoted cTAR/dTAR annealing (37). Both the fast and slow pathways are based on a distinct cTAR/huPrP(23–110)



Scheme 1. IC1 and IC2 represent intermediate complexes formed during the fast and slow pathway, respectively. The values of the $K_{M1,2}$ and $k_{f1,2}$ parameters (Table 1) determined from the fits of Supplementary Figure S1B were found to be close to the corresponding values reported for the HCV core protein in the same system, strengthening the similarity between the mechanisms of huPrP(23–110)- and HCV core-promoted cTAR/dTAR annealing reaction.

complex (cTAR_{1,2}) and involve a rate-limiting interconversion step ($k_{f1,2}$) coupled to a much faster, preceding binding step, governed by an equilibrium constant ($K_{M1,2}$).

To further characterize the two pathways, the effect of the sequence and stability of the oligonucleotides on the huPrP(23–110)-promoted cTAR/dTAR annealing kinetics was analysed. In this respect, dTAR was first substituted by the dTAR T-L mutant where the 6 nt of the loop were changed to T residues, thus preventing its base-pairing with the cTAR loop. These nucleotide substitutions did not significantly change the time course of ED formation, indicating that loop–loop interactions do not play a significant role (Supplementary Figure S1B and Supplementary Data). Furthermore, to investigate the role of the cTAR stem in the annealing reaction, we used the cTAR1.2 derivative where bases complementary to the bulged bases at Positions 49 and 52 have been introduced in order to stabilize the lower half of the stem. The annealing of this mutant to dTAR in the presence of huPrP(23–110) was extremely slow (Supplementary Figure S1C and Supplementary Data), indicating that both kinetic pathways of the huPrP(23–110)-promoted cTAR/dTAR annealing reaction are nucleated through the stems of cTAR and dTAR.

The nature of the two pathways was further investigated by analyzing the temperature dependence of the k_{obs} values (Supplementary Figure S1D and Supplementary Data) using the Arrhenius equation:

$$k_i = A_i \exp\left(\frac{E_{a,i}}{RT}\right) \quad (2)$$

where the rate constant k_i is given by $k_{\text{obs}}/[\text{dTAR}]$, A_i is the pre-exponential Arrhenius factor, $E_{a,i}$ is the activation energy, R is the universal gas constant, and T is the temperature (in Kelvin).

The temperature dependence of huPrP(23–110)-promoted cTAR/dTAR annealing provided positive enthalpy values for the transition state of 8.3 (± 0.7) kcal/mol and 16.5 (± 1) kcal/mol for the fast and slow pathways, respectively. These values indicated that cTAR/dTAR annealing promoted by the huPrP(23–110) peptide involves premelting of ~ 2 and 4 bp, for the fast and slow pathways, respectively (50,51). Moreover, the amplitude of the fast component was found to continuously increase with temperature, as observed for the HCV core (37).

Activation of DNA strand exchange by recombinant PrPs

The strand exchange assay (26) is designed to evaluate the ability of the chaperone protein to facilitate formation of the most stable nucleic acid conformation. It utilizes three DNA molecules, namely the wild-type plus strand, (+) wt (³²P-labelled), the wild-type minus strand, (–) wt, and the mutated minus strand, (–) mut. DNA molecules (+) wt and (–) wt are complementary, whereas (–) mut is only partially complementary to (+) wt (see scheme in Figure 2A). DNA molecules (+) wt and (–) mut are first heat annealed, giving rise to a double-stranded molecule containing mismatches. Then, DNA (–) wt and either PrP, or NCp7 as the positive control, were added to the pre-formed double-stranded DNA [(+) wt:(–) mut] molecules and incubated for 5 min at 37°C (see ‘Materials and Methods’ section). Last, nucleic acids were deproteinized and analysed by PAGE under native conditions. The strand exchange activity of the chaperone protein facilitates formation of the perfect double-stranded DNA [(+) wt:(–) wt] molecules at the expense of [(+) wt:(–) mut] molecules with mismatches (Figure 2A). If the recombinant PrPs have general nucleic acid chaperoning activities, they should facilitate formation of the most stable duplex and thus activate the substitution of DNA (–) wt for (–) mut in the double-stranded nucleic acid molecule (Figure 2A).

The ³²P-labelled DNA (+) wt is shown in lane 1 while control double-stranded DNA [(+) wt:(–) wt] and [(+) wt:(–) mut] are shown in lanes 3 and 4, respectively (Figure 2B). Addition of DNA (–) wt to double stranded [(+) wt:(–) mut] and incubation for 30 min at 0°C (lane 5) or 37°C (lane 6) did not result in any strand exchange. Addition of HIV-1 NCp7 together with DNA (–) wt resulted in a nearly complete strand exchange under the conditions where NCp7 to nucleotide molar ratios were 1/12 nt and 1/6 nt (lanes 7 and 8, respectively). Mutant NC(12–53) lacking the N- and C-terminal amino acids has only limited strand exchange activity (lanes 9 and 10). HuPrP was found to strongly activate the strand exchange (lanes 11 and 12). A polypeptide representing the N-terminal disordered region of huPrP, huPrP(23–145) (52), also exhibited a strong strand exchange activity (lanes 13 and 14), whereas the polypeptide huPrP(122–231), representing the C-terminal, well-folded region of huPrP (52,53), had little activity (lanes 15 and 16). The recombinant ovine PrP (ovPrP) behaved in a manner similar to huPrP, showing a strong strand exchange activity (lanes 17 and 18) at protein to nucleotide ratios of 1:12 and 1:6.

For kinetic analysis, DNA strand exchange assays were performed at 30°C from one to several minutes with NC, huPrP and ovPrP proteins at a protein to nucleotide molar ratio of 1/12 nt (see ‘Materials and Methods’ section). For the wild-type NCp7, the exchange rate at 30°C was 0.031 mol of DNA exchanged per mole of protein per minute. For the mutant NC(12–53), this value was reduced about nine times, but still was about three times higher than that observed in the absence of NC protein. The exchange rates for the recombinant PrPs were very close to that for NCp7 (0.025, 0.03 and 0.03 mol of DNA

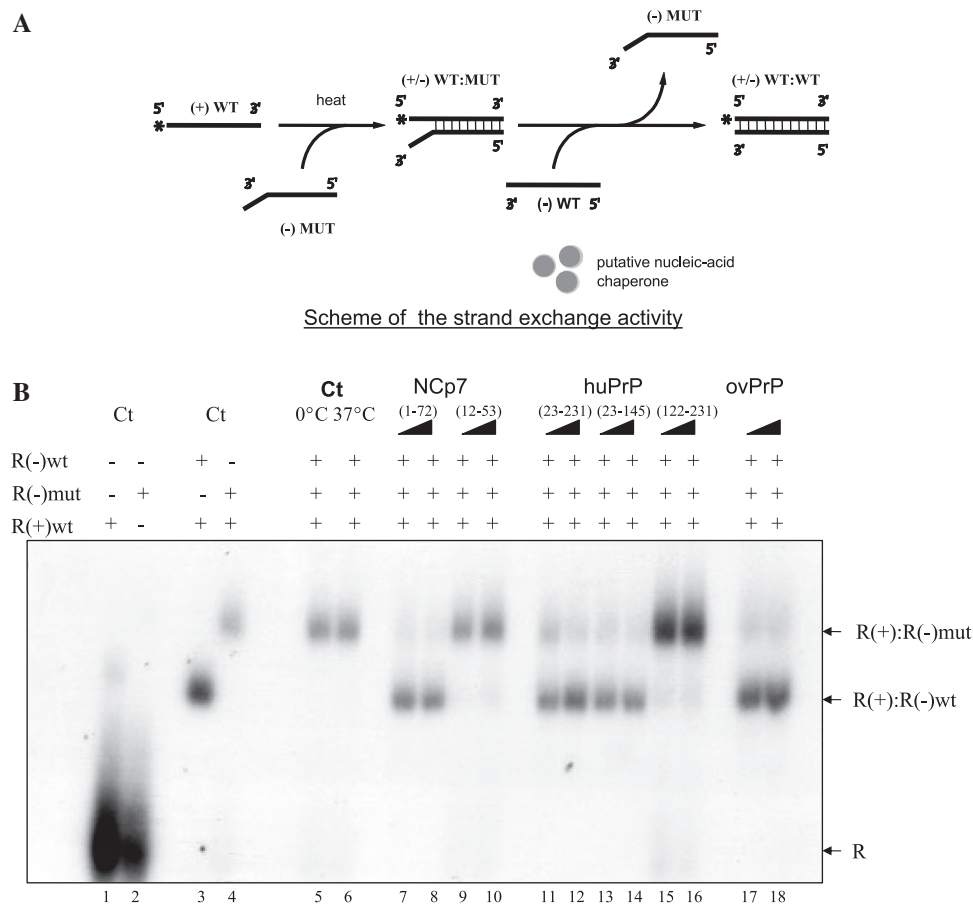


Figure 2. Facilitation of DNA strand exchange by PrPs. **(A)** Assay schematic. DNA sequences representing the R region of HIV-1 are 96nt in length. 5' ³²P-labelled R(+) wt was hybridized to R(-) mut to generate a double-stranded DNA with mismatches at the 3'-end (step 1). Fully complementary R(-) wt was added in the presence or absence of HIV-1 NCp7 or PrP (step 2). Strand exchange is visualized by native PAGE. **(B)** Assays with 3×10^{-9} M each of the DNA oligonucleotides were carried out at 37°C in 10 μ l (see 'Materials and Methods' section). Analysis of the reaction products was by 6% PAGE under native conditions. *R = ³²P-labelled DNA. Lanes 1 and 2: *R(+) wt alone and with R(-) mut at 0°C. Lanes 3 and 4: *R(+) hybridized to R(-) wt and *R(+) hybridized to R(-) mut. Lanes 5 and 6: *R(+):R(-) mut incubated with R(-) wt at 4 and 37°C for 30 min. Lanes 7–18: 5 min incubations with *R(+):R(-) mut and R(-) wt and with NCp7 (lanes 7 and 8), NC(12–53) (lanes 9 and 10), recombinant huPrP (lanes 11 and 12), huPrP(23–145) (lanes 13 and 14), huPrP(122–231) (lanes 15 and 16) or ovine PrP (lanes 17 and 18) at 6×10^{-8} M (protein to nucleotide molar ratio of 1/12) (odd lanes) or 12×10^{-8} M (protein to nucleotide molar ratio of 1/6) (even lanes). Proteins are indicated at the top of the figure; double-stranded products [*R(+):R(-) wt] and [*R(+):R(-) mut] are indicated on the right. Arrow is direction of electrophoresis. Note that the C-terminal region of huPrP is inactive (lanes 15 and 16).

per mole of protein per minute at 30°C for huPrP, huPrP(23–145) and ovPrP, respectively. For huPrP(122–231), the value was ~ 10 times lower than that for huPrP(23–145).

Strand exchange assays have also been carried out with cellular hnRNP A1 and p50, two well-characterized RNA chaperone proteins (40–42). Both proteins proved to facilitate the strand exchange reaction, although at a rate about three times lower than that observed under the present experimental conditions for huPrP (data not shown).

Facilitation of ribozyme-directed cleavage of an RNA substrate by PrPs

Next, we used the hammerhead ribozyme-directed cleavage of an RNA substrate to examine both the RNA annealing and unwinding activities of nucleic acid chaperones (27,28). Nucleic acid chaperones are thought

to enhance the rate of ribozyme cleavage by activating the annealing of the substrate RNA to the ribozyme (Figure 3A, step 1) and the unwinding and release of the cleaved RNA products (Figure 3A, step 3), thus allowing recycling of the ribozyme. The ribozyme cleavage assay aims at examining whether PrP accelerates ribozyme cleavage of an RNA substrate in a manner similar to the viral NCp7 chaperone (Figure 3A) (27,28). We selected the R3 hammerhead ribozyme and two RNA substrates, namely S14, with a 14nt substrate–ribozyme duplex length (7 nt either side of the cleavage site) and S20, with 10 nt either side of the cleavage site (28). The above RNA substrate model system was chosen due its likely biological relevance as evidenced by the similarity of data obtained both *in vitro* and in cultured cells (28). ³²P-labelled RNA S14, the ribozyme and PrP were mixed and incubated for 30 min. RNAs were deproteinized, recovered and analysed by PAGE under denaturing conditions. In the absence of

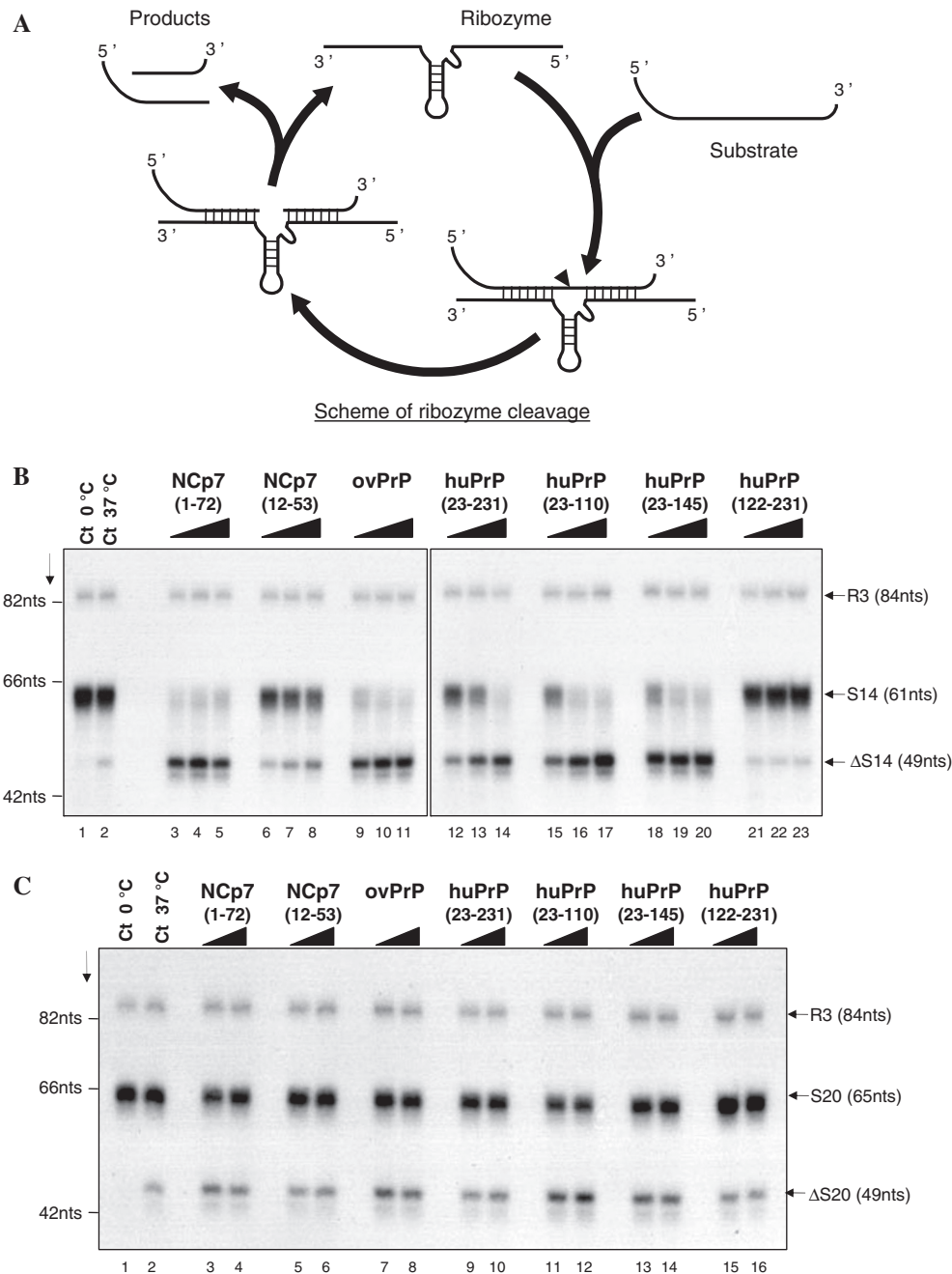


Figure 3. PrPs facilitate ribozyme cleavage of an RNA. (A) Assay schematic. A hammerhead ribozyme and a ^{32}P -labelled RNA substrate were generated by *in vitro* transcription and gel purified. Cleavage of the ^{32}P -RNA by the ribozyme appears to first necessitate hybridization of the ribozyme to the substrate (step 1). After RNA cleavage (step 2), the products must be released to allow recycling of the ribozyme (step 3). At the end of the reaction RNAs were deproteinized and analysed by PAGE under denaturing conditions to visualize the ^{32}P -RNA products. In the absence of a nucleic acid chaperone, hybridization of the RNA to the ribozyme and release of the products appear to be slow. Addition of a nucleic acid chaperone will accelerate hybridization of the substrate to the ribozyme and dissociation of the products and thus ribozyme turnover. Base pairing between the RNA substrate and ribozyme R3 are underlined on the substrate sequence. Ribozyme mediated cleavage occurs on the 3' side of A (space). For RNA S14, ...GAUUAAGUAGUA AGAGUGUCUGCA3', for RNA S20, ...GAUUAAGUAGUA AGAGUGUCUGCA3'. (B) Ribozyme-directed cleavage of RNA substrate S14. A 1×10^{-8} M of ribozyme R3 and 5×10^{-9} M of RNA S14 were incubated as described in the methods. ^{32}P -RNA substrate (S14) and product (ΔS14) were analysed by denaturing 8% PAGE. Lanes 1 and 2: R3 and S14 at 4 or 37°C. Lanes 3 and 5: HIV-1 NCp7 at NC concentrations of 2×10^{-8} , 4×10^{-8} and 8×10^{-8} M (protein/nt molar ratios of 1/20, 1/10 and 1/5). Lanes 6–8: NC(12–53) at concentrations of 1.6×10^{-7} , 3.2×10^{-7} and 6.4×10^{-7} M (molar ratios of 1/2.5, 1/1.2 and 1/0.6). Lanes 9–11: ovPrP at 2×10^{-8} , 4×10^{-8} and 8×10^{-8} M, respectively. Lanes 12–14: huPrP at concentrations of 2×10^{-8} , 4×10^{-8} and 8×10^{-8} M, respectively. Lanes 15–17: huPrP(23–110) at concentrations of 2×10^{-8} , 4×10^{-8} and 8×10^{-8} M, respectively. Lanes 18–20: huPrP(23–145) at concentrations of 2×10^{-8} , 4×10^{-8} and 8×10^{-8} M, respectively. Lanes 21–23: huPrP(122–231) at concentrations of 2×10^{-8} , 4×10^{-8} and 8×10^{-8} M, respectively. R3, S14 and the 5' sequences of S14 (ΔS14) are identified on the right. Markers are on the left. Arrow shows direction of electrophoresis. Note that the RNA products rapidly accumulate in the presence of a chaperone whereas they do not in the absence of a chaperone. (C) Ribozyme cleavage of RNA S20. Conditions were as in Figure 3B except that the substrate was S20 and protein concentrations of 4×10^{-8} (odd lanes) and 8×10^{-8} M (even lanes) were used. Proteins are identified at the top of the figure. R3, S20 and the 5' sequences of S20 (ΔS20) are identified on the right. Markers are on the left. Arrow shows direction of electrophoresis. Note that ribozyme-directed cleavage of S14 or S20 did not occur at 4°C (lane 1). Note that enhanced ribozyme cleavage by PrPs is probably via their match-maker activity for the annealing of S14 RNA to the hammerhead ribozyme (step 1) and their destabilizing activity upon S14 RNA cleavage (Step 3) [see ref. (25)].

a chaperone, ribozyme-directed cleavage of the RNA substrate occurred only slowly at 37°C (Figure 3B, lanes 1 at 4°C and 2 at 37°C; ³²P-RNA substrate is S14 and cleaved product ΔS14). In agreement with previous reports (28), HIV-1 NCp7 facilitated ribozyme cleavage of RNA S14 to reach completion at a concentration as low as 2×10^{-8} M (lanes 3–5). On the other hand, NC(12–53) was relatively inactive even at a concentration above 1×10^{-7} M (lanes 6–8). Interestingly, PrP of ovine or human origin showed strong enhancement of ribozyme cleavage at $2\text{--}4 \times 10^{-8}$ M (lanes 9–11 and 12–14, respectively). The N-terminal region of huPrP was very active (lanes 15–17 and 18–20) while the C-terminal region was very poorly active (lanes 21–23).

We also examined the effect of PrP using the RNA substrate S20, capable of forming an ED of 20 nt with the hammerhead ribozyme (Figure 3A) which precludes activation of ribozyme cleavage by HIV-1 NCp7 or hnRNP A1 (28). In the absence of NCp7 or PrP, only minimal ribozyme-directed cleavage of RNA S20 was observed at 37°C (Figure 3C, lane 2; ³²P-RNA substrate is S20 and product ΔS20) as seen with RNA S14 (Figure 3B, lane 2). The enhancement of ribozyme cleavage of RNA S20 by NCp7 remained very modest even at NCp7 concentration of 4×10^{-8} M (Figure 2C, lanes 3–4), in agreement with reported data (28). Mutant NC (12–53) was also very poorly active (lanes 5–6). The ovPrP and huPrP also exhibited very little, if any, activity using RNA S20 [lanes 7–8, 9–10, 11–12 and 13–14, for ovPrP, huPrP, huPrP(23–145) and huPrP(122–231), respectively].

Kinetic assays of ribozyme cleavage of RNA S14 were performed with NCp7, huPrP and ovPrP at a concentration of 4×10^{-8} M and cleavage monitored for up to 30 min. Initial rates were 10–12 μmol of RNA S14 cleaved at 37°C/min/mol of NCp7 and ovPrP. For huPrP, the observed rate was 3-fold slower, while it was approximately 100-fold slower for NC(12–53) at concentrations above 1×10^{-7} M, although two to three times above rates obtained in the absence of NC or PrP. Similar results were obtained at huPrP or NC concentration of 1×10^{-7} M (data not shown).

HuPrP and ovPrP facilitate RNA *trans*-splicing

To further examine the RNA chaperoning activity of the mammalian PrPs, we used the previously established *trans*-splicing assay (29,30) (Figure 4A), where the pre-mRNA of the thymidylate synthase (td) gene containing a group I intron was split into two halves. The first RNA transcript, H1, corresponds to the 5' exon sequence of 549 and 131 nt of the intron while the second RNA transcript, H2, represents the 3' part of the intron (147 nt) and part of exon 2 (23 nt) (Figure 4A). The two RNAs were ³⁵S-UMP labelled during transcription and were incubated together. Reaction was started by adding ³²P-GTP, so that the resulting spliced RNA was doubly labelled, internally and at the 5'-end with ³²P-GTP (Figure 4A). In the absence of protein, the reaction was carried out at 55°C to allow a productive interaction between H1 and H2 RNAs. *Trans*-splicing was indeed found to take place at 55°C but only to a

limited extent [data not shown and (36)] but not at 37°C according to the accumulation of the ³²P-GTP-II final product (lane 1 in Figure 4B and C). As previously reported (36) HIV-1 NCp7 strongly stimulated accumulation of ³²P-GTP-II and therefore *trans*-splicing (lanes 2–5), with an optimal enhancement at a concentration of 8×10^{-7} M (panel B, lane 4). Mutant NC(12–53) was found to be poorly active even at 2×10^{-6} M (panel B, lane 7).

The recombinant huPrP was found to be a strong activator of *trans*-splicing (Figure 4B, lanes 8–11), with an optimal activation at a concentration of 4×10^{-7} M (lanes 10 and 11). Interestingly the N-terminal huPrP peptide (23–144) also activated *trans*-splicing (Figure 4B, lanes 9–12) at concentrations of $2\text{--}4 \times 10^{-7}$ M (lanes 13 and 14) while the C-terminal domain (123–231) was clearly inactive (lanes 16 and 17) under the present conditions. The ovine PrP was already active at a concentration of 2×10^{-7} M (lanes 7–11 in panel C) and the N-terminal huPrP peptide (23–110) was as active as the full length huPrP (compare lanes 2–6 and 12–16 in panel C).

Inhibition of huPrP chaperoning activity by a thioaptamer

In a search for PrP-chaperoning inhibitors, we used a 12-nt long thioaptamer (GA-12; GACACAAGCCGA), with five modifications 5' to the dA residues, since it was found to bind with high affinity to Syrian hamster, bovine and human PrPs *in vitro* (32). We also selected a 11-nt 2' *O*-methyl oligoribonucleotide (mODN-11; GGUUUUUG UGU) because it was shown to be a potent inhibitor of the nucleic acid chaperoning activity of the HIV-1 nucleocapsid protein (31).

We examined the ability of these two selected oligonucleotides, namely GA-12 and mODN-11, and of a control ODN with the non-modified sequence GACACAAGCCGA (Ct-12) to inhibit the annealing activity of huPrP (Figure 5A and B). As shown in lanes 7–9, only GA-12 at 100–200 nM was able to completely inhibit huPrP annealing activity, while mODN-11 (lanes 4–6) and ODN Ct-12 (lanes 10–12) were poorly active. The impact of such ODNs on the hammerhead ribozyme directed cleavage of an RNA substrate was monitored under the same conditions. Again the thioaptamer GA-12 at 50–100 nM was found to extensively inhibit the RNA chaperoning of huPrP (lanes 7–9) while mODN-11 at 100–200 nM had moderate effect on huPrP (lane 6) and ODN Ct-12 had no effect (lanes 10–12). Last, we monitored the impact of these three ODNs on the *trans*-splicing reaction facilitated by huPrP, and again the thioaptamer GA-12 was efficiently (lanes 7–9) inhibiting *trans*-splicing activation by huPrP, while Ct-12 and mODN-11 were inactive (lanes 4–6 and 10–11). Results obtained with ovPrP were very similar, namely an inhibition of ovPrP chaperoning activity by GA-12 at 100 nM but not by mODN-11 and Ct-12 (data not shown).

We also examined the effect of GA-12 and mODN-11 on huPrP(23–110)-promoted cTAR/dTAR annealing using FRET. Both GA-12 and mODN-11 decreased the kinetics of huPrP(23–110)-promoted cTAR/dTAR annealing but the decrease was more pronounced with

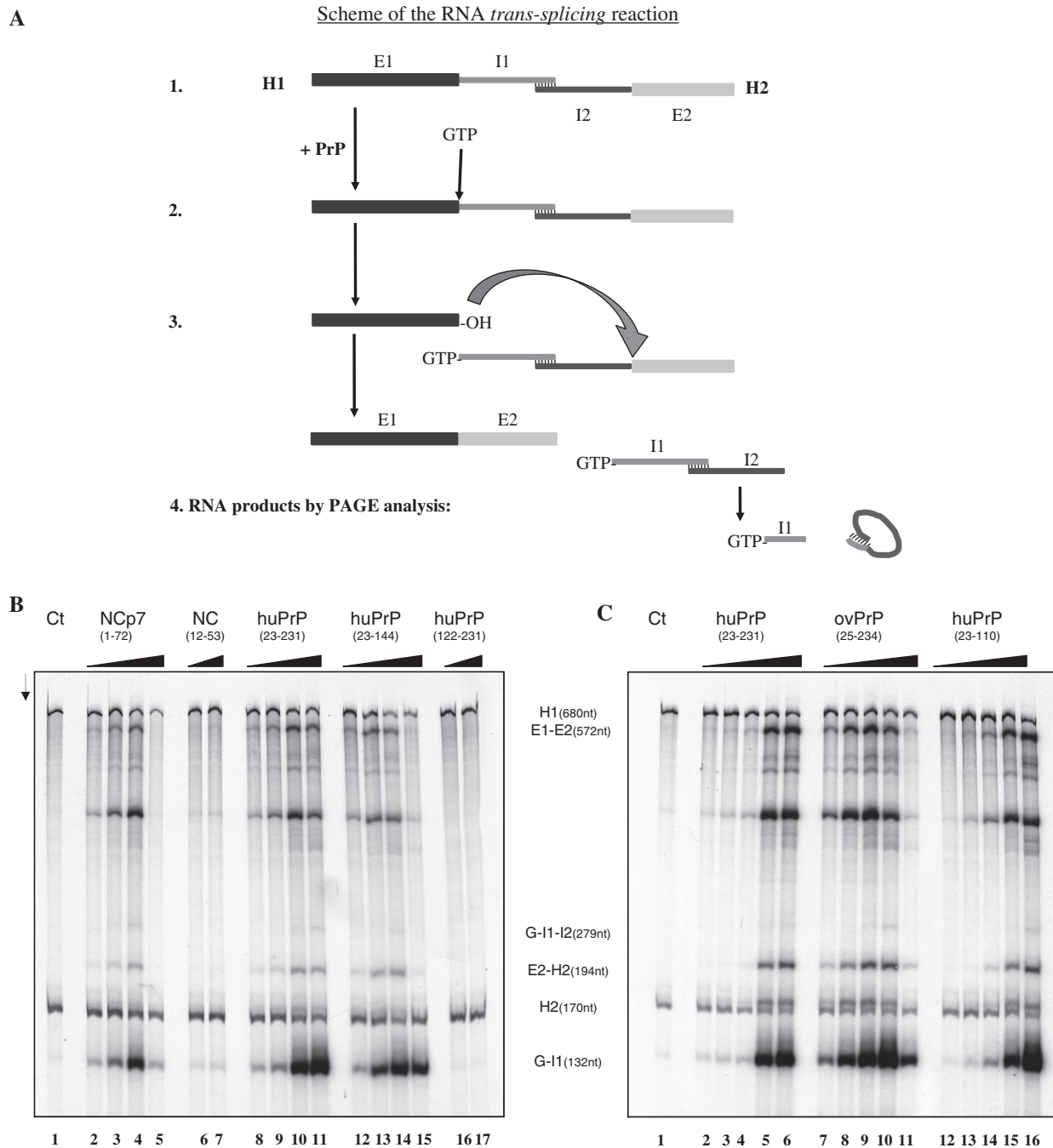


Figure 4. Facilitation of RNA *trans*-splicing by PrPs. (A) Schematic representation of the *trans*-splicing assay: the two RNA constructs H1 of 680 nt in length (encoding exon 1 of 549 nt and the 5' part of the intron of 131 nt) and H2 of 170 nt in length (encoding the 3' part of the intron of 147 nt and exon 2 of 23 nt) have to fold into a splicing competent structure (step 1). The splicing reaction was started upon addition of the ^{32}P -labelled GTP. The recombinant PrP was added at step 2, where indicated. The final RNA products are represented in step 4. All splicing rates were monitored based on the levels of the final product ^{32}P -labelled GTP-I1 [see (B)]. (B and C) Assays where the H1 and H2 RNAs were incubated with or without a nucleic acid chaperone, namely NCp7 or PrP. At the end of the reaction RNAs were phenol treated to remove the chaperone and analysed by PAGE in denaturing conditions (see 'Materials and Methods' section). The RNA substrates (H1, H2), the ligated exons (E1-E2) and the product (guanosine-5'-intron G-I1) are indicated. Panel B. Lane 1: *trans*-splicing reaction at 37°C with RNA alone at a concentration of 4×10^{-8} M. Lanes 2–5: HIV-1 NCp7 at concentrations of 2.5, 5, 10 and 20×10^{-7} M, corresponding to protein to nucleotide ratios of 1:128, 1:64, 1:32 and 1:16. Lanes 6 and 7: NC(12–53) at concentrations of 1 and 2×10^{-6} M, corresponding to peptide to nucleotide ratios of 1:32 and 1:16. Lanes 8–11: recombinant huPrP(23–231) at concentrations of 2, 4, 8 and 16×10^{-7} M, corresponding to PrP to nucleotide molar ratios of 1:160, 1:80, 1:40 and 1:20. Lanes 12–15: N-terminal huPrP(23–144) at the same protein to nucleotide ratios as for the huPrP(23–231). Lanes 16 and 17: C-terminal huPrP(123–231) at protein to nt molar ratios of 1:40 and 1:20. Panel C. Lane 1: splicing reaction at 37°C with RNA alone at a concentration of 4×10^{-8} M. Lanes 2–6: huPrP at concentrations of 1, 2, 4, 8 and 16×10^{-7} M. Lanes 7–11: recombinant ovPrP at concentrations of 2, 4, 8, 16 and 32×10^{-7} M. Lanes 12–16: huPrP(23–110) at concentrations of 1, 2, 4, 8 and 16×10^{-7} M. Note that HIV-1 NCp7, huPrP and ovPrP strongly activated *trans*-splicing at protein to nt molar ratios of 1:20 to 1:40. Peptides NC(12–53) and C-terminal huPrP(122–231) were very poorly active (lanes 6, 7, 16, 17; in panel B).

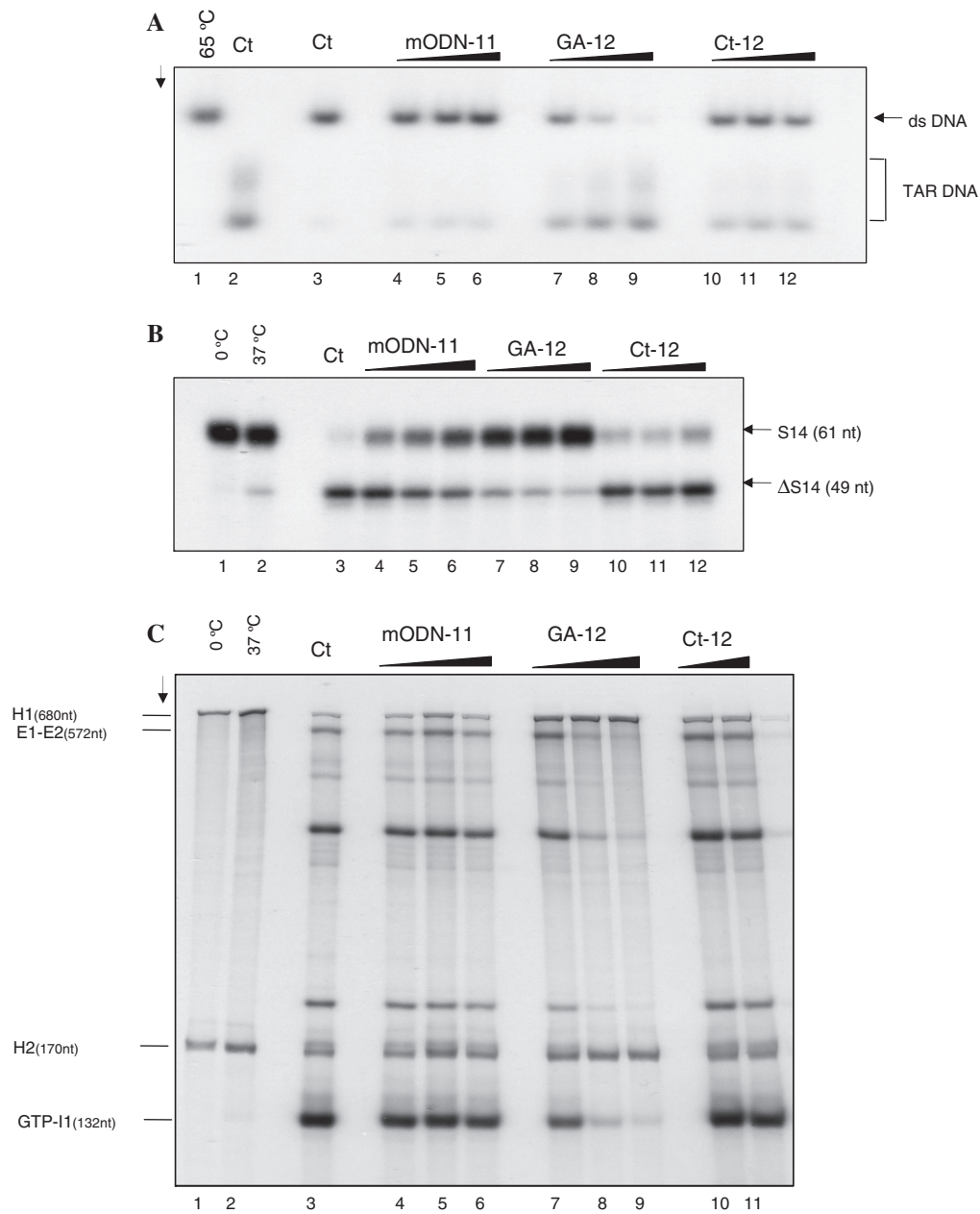


Figure 5. Thioaptamer inhibition of huPrP chaperoning activities *in vitro*. **(A)** Annealing of TAR(+)/TAR(-). The annealing conditions were exactly as described in the 'Materials and Methods' section with the TAR(+) and TAR(-) DNA. PAGE analyses are described in 'Materials and Methods' section. Lane 1: Control at 65°C for 30 min; lane 2: at 37°C for 30 min. Lanes 3-12: with huPrP for 5 min at 37°C. Lane 3: control showing the complete hybridization of TAR(+) and TAR(-) DNA. Lanes 4-6: with mODN-11 added at the start of the incubation period at 50, 100 and 200 nM. No inhibition of huPrP annealing activity was observed. Lanes 7-9: with ODN GA-12 at 50, 100 and 200 nM. Note that ODN GA-12 causes a complete inhibition of huPrP chaperoning at 200 nM. Lanes 10-12: with control ODN Ct-12 at 50, 100 and 200 nM. **(B)** Ribozyme mediated cleavage of an RNA substrate. The conditions for the ribozyme cleavage were exactly as described in the 'Materials and Methods' section with hammerhead ribozyme and the RNA substrate. PAGE analyses under denaturing conditions are described in the 'Materials and Methods' section. Lane 1: Control at 0°C for 30 min; lane 2: at 37°C for 30 min without PrP. Lane 3: control with huPrP for 15 min at 37°C showing a complete cleavage. Lanes 4-6: with mODN-11 added at the start of the incubation period at 50, 100 and 200 nM. Some inhibition of huPrP activity was observed at 100 nM. Lanes 7-9: with ODN GA-12 at 50, 100 and 200 nM. Note that ODN GA-12 causes a nearly complete inhibition of huPrP at 50 nM and 100 nM for ovPrP (data not shown). Lanes 10-12: with control ODN Ct-12 at 50, 100 and 200 nM. **(C)** The RNA *trans*-splicing reaction. The conditions for the *trans*-splicing reactions were exactly as described in the 'Materials and Methods' section with the H1 and H2 RNAs. PAGE analyses under denaturing conditions are described in the 'Materials and Methods' section. Lane 1: Control at 0°C for 30 min; lane 2: at 37°C for 30 min without PrP. Lane 3: control with huPrP at 8×10^{-7} M for 30 min at 37°C showing a complete cleavage. Lanes 4-6: with mODN-11 added at the start of the incubation period at 50, 100 and 200 nM. No inhibition of PrP activity was observed. Lanes 7-9: with ODN GA-12 at 50, 100 and 200 nM. Note that ODN GA-12 causes a nearly complete inhibition of huPrP at 100 nM. Lanes 10-12: with control ODN Ct-12 at 50, 100 and 200 nM.

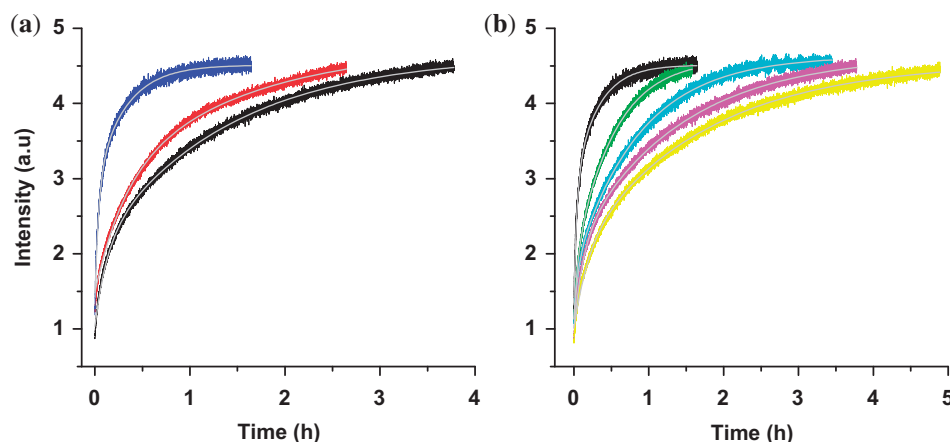


Figure 6. Inhibition of huPrP(23–110)-promoted cTAR/dTAR annealing. (A) Comparative effects of GA-12 and mODN-11. A 10 nM of doubly labelled cTAR was mixed with 300 nM of non-labelled dTAR at a peptide/oligonucleotide molar ratio of 1:1 in the absence (blue) and presence of GA-12 (black) and mODN-11 (red) sequences, added at five times molar excess, as compared to cTAR and dTAR. Excitation and emission wavelengths were 520 and 550 nm, respectively. The gray lines correspond to the fits of the kinetic traces to Equation (1) and the fitting parameters given in Supplementary Table S1A. (B) Concentration dependence of the effect of GA-12 on the annealing kinetics. Kinetic traces were recorded with 10 nM doubly labelled TMR-cTAR-F1 and 300 nM non-labelled dTAR in the absence (black) and the presence of GA-12, added at 0.25× (green), 1× (cyan), 5× (magenta) and 10× (yellow) molar ratio as compared to cTAR and dTAR concentrations. HuPrP(23–110) was added at a peptide/oligonucleotide ratio of 1:1. Excitation and emission wavelengths were 480 and 520 nm, respectively. All experiments were performed in 25 mM Tris-HCl (pH 7.5), 30 mM NaCl, 0.2 mM MgCl₂ at 20°C. The gray lines correspond to the fits of the kinetic traces to Equation (1) and the fitting parameters given in Supplementary Table S1B.

GA-12 (Figure 6A). Finally, we analysed the concentration dependence of the inhibition of GA-12 on the huPrP-promoted annealing of cTAR/dTAR (Figure 6A). The inhibitory effect of GA-12 increased with its concentration and appeared already when the GA-12 concentration was one order of magnitude lower as compared to cTAR and dTAR concentrations. All kinetic traces in the presence of GA-12 were adequately fitted with Equation (1) and showed a decrease in both $k_{\text{obs}1}$ and $k_{\text{obs}2}$ values (Supplementary Table S1a and S1b). These data are consistent with a tight binding of GA-12 to huPrP, which reduces the concentration of huPrP available for promoting the cTAR/dTAR annealing reaction. The inhibitor was also found to decrease the amplitude of the fast pathway, further substantiating the hypothesis of a huPrP sequestration by the inhibitor, since a similar decrease in the amplitude of the fast pathway with the concentration of protein was observed with the HCV core protein (37).

Taken together these results show that the GACACAA GCCGA thioaptamer is a potent inhibitor of the huPrP nucleic acid chaperoning activity *in vitro* and this appears to rely on the backbone modifications.

DISCUSSION

Collectively the data presented herein clearly show that the human and ovine PrPs can assist the folding of RNA and DNA molecules in physiological conditions and at concentrations of 10^{-7} M or below (Figures 1–5). Thus, these two mammalian PrPs have the hallmarks of *bona fide* nucleic acid chaperones (24,25). In addition, the chaperoning properties of the human PrP reside within the N-terminal region of the protein (Figures 1–4).

Interestingly this N-terminal region possesses the characteristic features of a chaperone (54,55) since it contains aromatic residues and clusters of basic amino acids in an intrinsically unstructured environment (52,56,57). Despite the absence (or relaxation) of structural constraints on mutations in the N-terminal domain of PrP, the sequence and distribution of basic amino acids is highly conserved between various mammalian PrPs (data not shown).

As a consequence of its chaperone activity, the N-terminal region of huPrP was found to activate by two orders of magnitude the kinetics of the cTAR/dTAR annealing reaction, probably through a reaction mechanism similar to that described for the HCV core protein (37). In this mechanism, the fast and slow pathways were found to be nucleated through the cTAR ends, but differ by the number of base pairs that should be premelted in the original cTAR secondary structure to nucleate the IC formation. In its free form, as a consequence of the thermal fraying that occurs spontaneously at room temperature, the closed cTAR species was shown to be in equilibrium with partially melted cTAR species where either the terminal or both the terminal and penultimate double-stranded segments of the stem are melted (47–49). In this respect, the 8.3 kcal/mol enthalpy energy associated to the fast pathway is consistent with the melting of the terminal double-stranded 3-bp segment, which is poorly stable due to its position at the end of the stem and the presence of the neighbouring G52 bulge. On the other hand, the 16.5 kcal/mol enthalpy energy associated with the slow pathway is consistent with the energy needed to melt both the terminal and penultimate double-stranded segments of the cTAR stem (Figure 7). As a consequence of this thermal fraying, the

PrP-bound cTAR₁ species in the fast pathway is thought to form IC1, stabilized by the seven intermolecular base pairs resulting from the annealing of both the 3' and 5' terminal strands of cTAR with the complementary terminal strands of dTAR. Since the K_M values of IC1 and IC2 are similar, we suggest that the PrP-bound cTAR₂ species in the slow pathway anneals only through one of its frayed strands with the complementary

dTAR sequence to form IC2, also stabilized by 7 bp. Further conversion of both ICs into the ED most probably relies on the conformational rearrangement and melting of the stable upper part of both TAR species (58–61). As for the core protein of the hepatitis C virus (HCV) (37,62,63), the interconversion rate of IC1 into ED was found to be much larger than for IC2 (Table 1), probably as a consequence of the more

Table 1. Comparison of the kinetic parameters of the huPrP(23–110)- and HCV core-promoted cTAR/dTAR annealing^a

	K_{M1} (M^{-1}) ($\times 10^{-6}$)	K_{M2} (M^{-1}) ($\times 10^{-6}$)	k_{f1} (s^{-1}) ($\times 10^2$)	k_{f2} (s^{-1}) ($\times 10^2$)
HuPrP	2.2 (± 0.8)	1.5 (± 1)	1.1 (± 0.1)	0.15 (± 0.03)
HCV Core ^b	4 (± 2)	1.4 (± 0.7)	4.5 (± 0.9)	1.6 (± 0.2)

^aThe equilibrium and kinetic constants for HuPrP-promoted cTAR/dTAR annealing reaction are calculated, as described in Supplementary Figure S1B.

^bData from (37) in the same buffer, with a core/oligonucleotide molar ratio of 1.4.

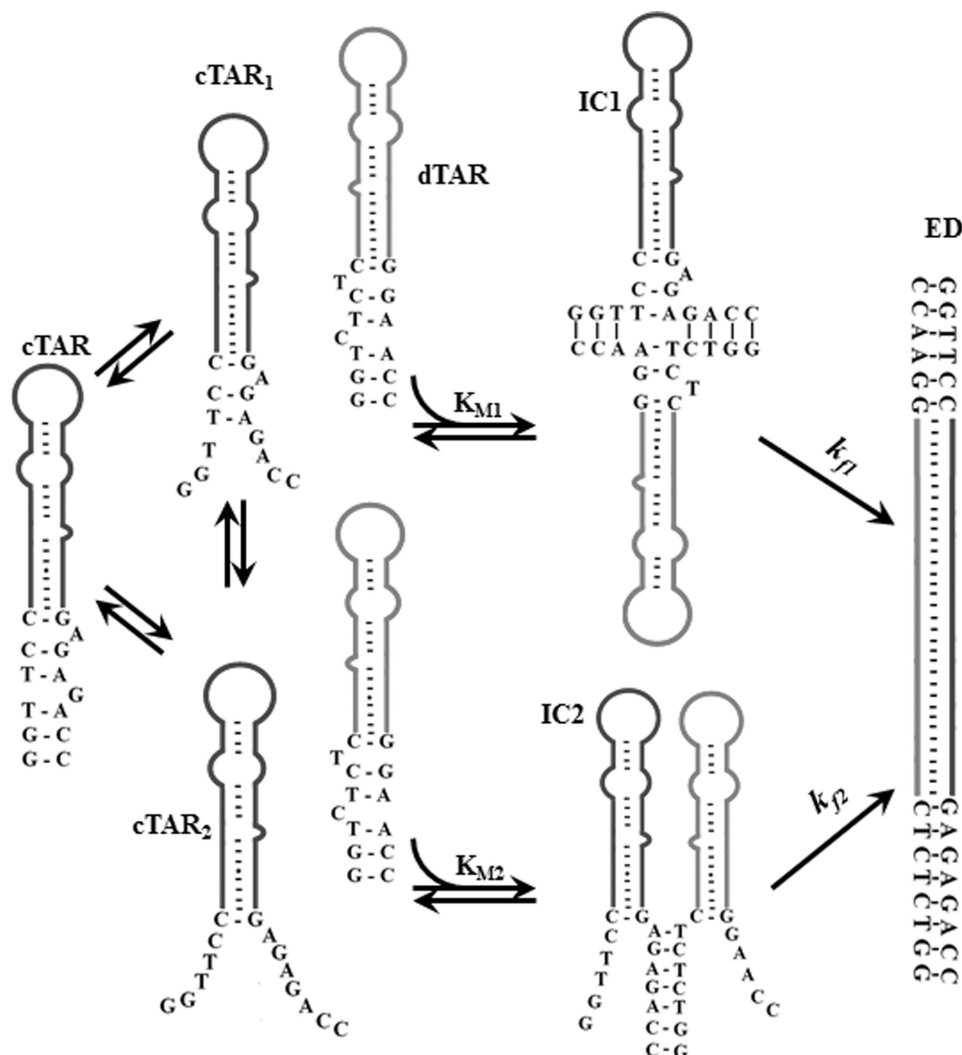


Figure 7. Proposed mechanism for PrP-promoted cTAR/dTAR annealing. The two pathways of the annealing reaction are thought to rely on the thermal fraying of cTAR that leads to a fast equilibrium (microseconds range) between the premelted cTAR species (cTAR₁ and cTAR₂) (47). The upper and lower pathways are associated with the fast and slow kinetic components, respectively. In both pathways, the cTAR species nucleate an intermediate complex (IC) through the stem termini. Then, the ICs are converted in a rate-limiting step into the final extended duplex (ED).

favorable zippering mechanism adopted by IC1 as compared to the invasion mechanism adopted by IC2 (Figure 7).

With respect to NCp7, the natural partner of HIV-1 cTAR and dTAR sequences, data revealed that the equilibrium constant K_M for IC formation was two orders of magnitude lower for the N-terminal region of huPrP than for NCp7 added at a ratio of 10 peptides per oligonucleotide ($K = 10^8 \text{ M}^{-1}$) (64). This difference may in part be explained by the incomplete coating of the oligonucleotides by huPrP(23–110), since the K_M value of the IC was shown to be strongly dependent on the level of protein coating in the case of NCp7 (with about three orders of magnitude difference between low and full coating). Interestingly, the interconversion rate value of the fast pathway for the N-terminal region of huPrP was close to the value (0.03 s^{-1}) of the corresponding parameter obtained with NCp7. The comparison of this parameter for the two proteins is more straightforward, since this parameter was found to be only poorly dependent on the level of NCp7 coating (64). Thus, huPrP(23–110) appears to promote the conversion of IC1 to the final ED with the same efficiency as NCp7. Moreover, as for NCp7 (35,64,65), huPrP(23–110) was found to nucleate the cTAR/dTAR annealing reaction through the stems of cTAR and dTAR but without destabilization of the termini (Figure 1, inset). As for the HCV core protein, this is a likely consequence of the stronger ‘nucleic acid aggregating’ properties of the huPrP peptide that compensate for the absence of its destabilizing activity. This propensity of the huPrP N-terminal peptide to efficiently neutralize the negatively charged oligonucleotides and promote their aggregation is probably related to the more flexible nature of this peptide, as compared to NCp7 with the structured zinc fingers (66,67).

It is hypothesized that such a disorder status of the N-terminal domain of PrP allows for the recognition of a rather large number of cellular and viral RNA sequences, as well as protein partners, as amply shown for the cellular protein FMRP and the retroviral NC proteins [reviewed in (54)]. Recognition of many partners by nucleic acid chaperones favours the notion that these ubiquitous proteins can achieve several functions as exemplified by retroviral NC proteins in virus structure, genome replication and virus assembly [reviewed in (68,69)] and the cellular p53 and p50 proteins in DNA maintenance and mRNA translation, respectively (40,70).

What is the function of PrP and what could be its role as an RNA chaperone? For a long time the physiological function of PrP^C remained a matter of speculation and debate. Recent data demonstrated that PrP is involved in cell–cell adhesion whereby it controls cell movements in the early gastrula of zebrafish embryos [reviewed in (71)]. In addition, PrP appears to trigger cellular signalling via Src-related kinases especially in neurons (18). These cellular functions of PrP could well be linked to the fact that PrP is, at least in part, a membrane associated protein through its GPI anchor or its transmembrane domain [reviewed in (72)]. Regarding the RNA chaperoning activity, PrP could act at the level of mRNA translation as shown for some fungal PrPs (73) and for the prion-like

neuronal protein CPEB (cytoplasmic polyadenylation element binding protein) (74). In agreement with this notion, we have recently found that a fraction of huPrP is associated with translating ribosomes in human cells, impacting on mRNA translation notably in cells in the G2M phase (to be published elsewhere). Thus PrP would be another chaperone protein associated with the cellular translation machinery (Supplementary Figure S2), thereby regulating the level of mRNA translation in a manner similar to other essential RNA chaperones such as hnRNP A1 in every cell type and FMRP in neurons (to be published elsewhere). Indeed, formation of PrP^C aggregates and fibrils upon binding to small nucleic acid molecules would have a negative impact on translation and thus on the cell physiology (75,76), and might also be involved in the pathological conversion of PrP^C to the infectious form, ultimately facilitating prion propagation [(77,78), reviewed in (75,79)].

We also report that a small thioaptamer (GA-12) is capable of inhibiting the PrP chaperoning activity *in vitro* but not that of HIV-1 NC (data not shown). At the same time a small methylated oligoribonucleotide (mODN-11), previously found to be a potent inhibitor of HIV-1 NC *in vitro* and of HIV-1 replication in cells (31), had little inhibitory potential against PrP. Kinetic data suggest that the small thioaptamer functions by tightly binding to the N-terminal domain of huPrP. This in turn may cause the formation of a complex where the N-terminal disordered domain adopts a stable ordered conformation. Such thioaptamer derivatives were found to delay the onset of prion disease in the mouse model (80), most probably by binding to PrP^C, in turn preventing its recruitment into aggregates of PrP^{Sc}. These results and those recently published on HIV-1 NC pave the way for the future development of highly modified oligonucleotides to treat diseases caused by RNA viruses as well as by a non-conventional agent.

SUPPLEMENTARY DATA

Supplementary Data are available at NAR Online.

ACKNOWLEDGEMENTS

The authors thank W. Surewicz (USA) for huPrP, PrP(23–145) and PrP(123–231), C. Branlant (France) and L. Ovchinnikov (Russia) for hnRNP A1 and p50, respectively, E. Bertrand (France) and J. Rossi (USA) for pR3, pS14 and pS20. The authors also thank D. Ficheux (France) for NCp7 and NC(12–53).

FUNDING

ANRS, INSERM, GIS Prions (France) and TRIOH (FP6 EC). Funding for open access charge: INSERM, ANRS, CNRS (FRANCE).

Conflict of interest statement. None declared.

REFERENCES

- Weissmann, C. (2004) The state of the prion. *Nat. Rev. Microbiol.*, **2**, 861–871.
- Aguzzi, A., Baumann, F. and Bremer, J. (2008) The prion's elusive reason for being. *Annu. Rev. Neurosci.*, **31**, 439–477.
- Prusiner, S.B., Scott, M.R., DeArmond, S.J. and Cohen, F.E. (1998) Prion protein biology. *Cell*, **93**, 337–348.
- Basler, K., Oesch, B., Scott, M., Westaway, D., Walchli, M., Groth, D.F., McKinley, M.P., Prusiner, S.B. and Weissmann, C. (1986) Scrapie and cellular PrP isoforms are encoded by the same chromosomal gene. *Cell*, **46**, 417–428.
- Oesch, B., Westaway, D., Walchli, M., McKinley, M.P., Kent, S.B., Aebersold, R., Barry, R.A., Tempst, P., Teplow, D.B., Hood, L.E. *et al.* (1985) A cellular gene encodes scrapie PrP 27-30 protein. *Cell*, **40**, 735–746.
- Pan, K.M., Baldwin, M., Nguyen, J., Gasset, M., Serban, A., Groth, D., Mehlhorn, I., Huang, Z., Fletterick, R.J., Cohen, F.E. *et al.* (1993) Conversion of alpha-helices into beta-sheets features in the formation of the scrapie prion proteins. *Proc. Natl Acad. Sci. USA*, **90**, 10962–10966.
- Horwich, A.L. and Weissman, J.S. (1997) Deadly conformations—protein misfolding in prion disease. *Cell*, **89**, 499–510.
- Bueler, H., Aguzzi, A., Sailer, A., Greiner, R.A., Autenried, P., Aguet, M. and Weissmann, C. (1993) Mice devoid of PrP are resistant to scrapie. *Cell*, **73**, 1339–1347.
- Westergaard, L., Christensen, H.M. and Harris, D.A. (2007) The cellular prion protein (PrP^C): its physiological function and role in disease. *Biochim. Biophys. Acta*, **1772**, 629–644.
- Bueler, H., Fischer, M., Lang, Y., Bluethmann, H., Lipp, H.P., DeArmond, S.J., Prusiner, S.B., Aguet, M. and Weissmann, C. (1992) Normal development and behaviour of mice lacking the neuronal cell-surface PrP protein. *Nature*, **356**, 577–582.
- Steele, A.D., Lindquist, S. and Aguzzi, A. (2007) The prion protein knockout mouse: a phenotype under challenge. *Prion*, **1**, 83–93.
- Brown, D.R., Wong, B.S., Hafiz, F., Clive, C., Haswell, S.J. and Jones, I.M. (1999) Normal prion protein has an activity like that of superoxide dismutase. *Biochem. J.*, **344(Pt 1)**, 1–5.
- Milhavet, O., McMahon, H.E., Rachidi, W., Nishida, N., Katamine, S., Mange, A., Arlotto, M., Casanova, D., Riondel, J., Favier, A. *et al.* (2000) Prion infection impairs the cellular response to oxidative stress. *Proc. Natl Acad. Sci. USA*, **97**, 13937–13942.
- Brown, D.R., Qin, K., Herms, J.W., Madlung, A., Manson, J., Strome, R., Fraser, P.E., Kruck, T., von Bohlen, A., Schulz-Schaeffer, W. *et al.* (1997) The cellular prion protein binds copper in vivo. *Nature*, **390**, 684–687.
- Mouillet-Richard, S., Ermonval, M., Chebassier, C., Laplanche, J.L., Lehmann, S., Launay, J.M. and Kellermann, O. (2000) Signal transduction through prion protein. *Science*, **289**, 1925–1928.
- Chiari, L.B., Freitas, A.R., Zanata, S.M., Brentani, R.R., Martins, V.R. and Linden, R. (2002) Cellular prion protein transduces neuroprotective signals. *EMBO J.*, **21**, 3317–3326.
- Bounhar, Y., Zhang, Y., Goodyer, C.G. and LeBlanc, A. (2001) Prion protein protects human neurons against Bax-mediated apoptosis. *J. Biol. Chem.*, **276**, 39145–39149.
- Malaga-Trillo, E., Solis, G.P., Schrock, Y., Geiss, C., Luncz, L., Thomanetz, V. and Stuermer, C.A. (2009) Regulation of embryonic cell adhesion by the prion protein. *PLoS Biol.*, **7**, e55.
- Gabus, C., Derrington, E., Leblanc, P., Chnaiderman, J., Dormont, D., Swietnicki, W., Morillas, M., Surewicz, W.K., Marc, D., Nandi, P. *et al.* (2001) The prion protein has RNA binding and chaperoning properties characteristic of nucleocapsid protein NCP7 of HIV-1. *J. Biol. Chem.*, **276**, 19301–19309.
- Gabus, C., Auxilien, S., Pechoux, C., Dormont, D., Swietnicki, W., Morillas, M., Surewicz, W., Nandi, P. and Darlix, J.L. (2001) The prion protein has DNA strand transfer properties similar to retroviral nucleocapsid protein. *J. Mol. Biol.*, **307**, 1011–1021.
- Moscardini, M., Pistello, M., Bendinelli, M., Ficheux, D., Miller, J.T., Gabus, C., Le Grice, S.F., Surewicz, W.K. and Darlix, J.L. (2002) Functional interactions of nucleocapsid protein of feline immunodeficiency virus and cellular prion protein with the viral RNA. *J. Mol. Biol.*, **318**, 149–159.
- Leblanc, P., Baas, D. and Darlix, J.L. (2004) Analysis of the interactions between HIV-1 and the cellular prion protein in a human cell line. *J. Mol. Biol.*, **337**, 1035–1051.
- Lotscher, M., Recher, M., Lang, K.S., Navarini, A., Hunziker, L., Santimaria, R., Glatzel, M., Schwarz, P., Boni, J. and Zinkernagel, R.M. (2007) Induced prion protein controls immune-activated retroviruses in the mouse spleen. *PLoS ONE*, **2**, e1158.
- Schroeder, R., Barta, A. and Semrad, K. (2004) Strategies for RNA folding and assembly. *Nat. Rev. Mol. Cell. Biol.*, **5**, 908–919.
- Cristofari, G. and Darlix, J.L. (2002) The ubiquitous nature of RNA chaperone proteins. *Prog. Nucleic Acid Res. Mol. Biol.*, **72**, 223–268.
- Tsuchihashi, Z. and Brown, P.O. (1994) DNA strand exchange and selective DNA annealing promoted by the human immunodeficiency virus type 1 nucleocapsid protein. *J. Virol.*, **68**, 5863–5870.
- Tsuchihashi, Z., Khosla, M. and Herschlag, D. (1993) Protein enhancement of hammerhead ribozyme catalysis. *Science*, **262**, 99–102.
- Bertrand, E.L. and Rossi, J.J. (1994) Facilitation of hammerhead ribozyme catalysis by the nucleocapsid protein of HIV-1 and the heterogeneous nuclear ribonucleoprotein A1. *EMBO J.*, **13**, 2904–2912.
- Coetzee, T., Herschlag, D. and Belfort, M. (1994) Escherichia coli proteins, including ribosomal protein S12, facilitate in vitro splicing of phage T4 introns by acting as RNA chaperones. *Genes Dev.*, **8**, 1575–1588.
- Galloway Salvo, J.L., Coetzee, T. and Belfort, M. (1990) Deletion-tolerance and trans-splicing of the bacteriophage T4 td intron. Analysis of the P6-L6a region. *J. Mol. Biol.*, **211**, 537–549.
- Grigorov, B., Bocquin, A., Gabus, C., Avilov, S., Mély, Y., Agopian, A., Divita, G., Gottikh, M., Witvrouw, M. and Darlix, J.L. (2011) Identification of a methylated oligoribonucleotide as a potent inhibitor of HIV-1 reverse transcription. *Nucleic Acids Res.*, In press.
- King, D.J., Safar, J.G., Legname, G. and Prusiner, S.B. (2007) Thioaptamer interactions with prion proteins: sequence-specific and non-specific binding sites. *J. Mol. Biol.*, **369**, 1001–1014.
- Rezaei, H., Marc, D., Choiset, Y., Takahashi, M., Hui Bon Hoa, G., Haertle, T., Grosclaude, J. and Debey, P. (2000) High yield purification and physico-chemical properties of full-length recombinant allelic variants of sheep prion protein linked to scrapie susceptibility. *Eur. J. Biochem.*, **267**, 2833–2839.
- Gabus, C., Mazroui, R., Tremblay, S., Khandjian, E.W. and Darlix, J.L. (2004) The fragile X mental retardation protein has nucleic acid chaperone properties. *Nucleic Acids Res.*, **32**, 2129–2137.
- Godet, J., de Rocquigny, H., Raja, C., Glasser, N., Ficheux, D., Darlix, J.L. and Mely, Y. (2006) During the early phase of HIV-1 DNA synthesis, nucleocapsid protein directs hybridization of the TAR complementary sequences via the ends of their double-stranded stem. *J. Mol. Biol.*, **356**, 1180–1192.
- Kuciak, M., Gabus, C., Ivanyi-Nagy, R., Semrad, K., Storchak, R., Chaloin, O., Muller, S., Mely, Y. and Darlix, J.L. (2008) The HIV-1 transcriptional activator Tat has potent nucleic acid chaperoning activities in vitro. *Nucleic Acids Res.*, **36**, 3389–3400.
- Sharma, K., Didier, P., Darlix, J.L., de Rocquigny, H., Bensikaddour, H., Lavergne, J.P., Penin, F., Lessinger, J.M. and Mely, Y. (2010) Kinetic analysis of the nucleic acid chaperone activity of the hepatitis C virus core protein. *Nucleic Acids Res.*, **38**, 3632–3642.
- Herschlag, D. (1995) RNA chaperones and the RNA folding problem. *J. Biol. Chem.*, **270**, 20871–20874.
- Rajkowsch, L., Semrad, K., Mayer, O. and Schroeder, R. (2005) Assays for the RNA chaperone activity of proteins. *Biochem. Soc. Trans.*, **33**, 450–456.
- Skabkin, M.A., Evdokimova, V., Thomas, A.A. and Ovchinnikov, L.P. (2001) The major messenger ribonucleoprotein particle protein p50 (YB-1) promotes nucleic acid strand annealing. *J. Biol. Chem.*, **276**, 44841–44847.
- Portman, D.S. and Dreyfuss, G. (1994) RNA annealing activities in HeLa nuclei. *EMBO J.*, **13**, 213–221.

42. Herschlag, D., Khosla, M., Tsuchihashi, Z. and Karpel, R.L. (1994) An RNA chaperone activity of non-specific RNA binding proteins in hammerhead ribozyme catalysis. *EMBO J.*, **13**, 2913–2924.
43. Darlix, J.L., Lapadat-Tapolsky, M., de Rocquigny, H. and Roques, B.P. (1995) First glimpses at structure-function relationships of the nucleocapsid protein of retroviruses. *J. Mol. Biol.*, **254**, 523–537.
44. Rein, A., Henderson, L.E. and Levin, J.G. (1998) Nucleic-acid-chaperone activity of retroviral nucleocapsid proteins: significance for viral replication. *Trends Biochem. Sci.*, **23**, 297–301.
45. Ameres, S.L., Shcherbakov, D., Nikonova, E., Piendl, W., Schroeder, R. and Semrad, K. (2007) RNA chaperone activity of L1 ribosomal proteins: phylogenetic conservation and splicing inhibition. *Nucleic Acids Res.*, **35**, 3752–3763.
46. Rajkowitzsch, L., Chen, D., Stampf, S., Semrad, K., Waldsich, C., Mayer, O., Jantsch, M.F., Konrat, R., Blasi, U. and Schroeder, R. (2007) RNA chaperones, RNA annealers and RNA helicases. *RNA Biol.*, **4**, 118–130.
47. Azoulay, J., Clamme, J.P., Darlix, J.L., Roques, B.P. and Mely, Y. (2003) Destabilization of the HIV-1 complementary sequence of TAR by the nucleocapsid protein through activation of conformational fluctuations. *J. Mol. Biol.*, **326**, 691–700.
48. Beltz, H., Azoulay, J., Bernacchi, S., Clamme, J.P., Ficheux, D., Roques, B., Darlix, J.L. and Mely, Y. (2003) Impact of the terminal bulges of HIV-1 cTAR DNA on its stability and the destabilizing activity of the nucleocapsid protein NCp7. *J. Mol. Biol.*, **328**, 95–108.
49. Bernacchi, S., Stoylov, S., Piemont, E., Ficheux, D., Roques, B.P., Darlix, J.L. and Mely, Y. (2002) HIV-1 nucleocapsid protein activates transient melting of least stable parts of the secondary structure of TAR and its complementary sequence. *J. Mol. Biol.*, **317**, 385–399.
50. Cantor, C. and Schimmel, P. (1980) *Biophysical Chemistry Part 2: Techniques for the Study of Biological Structure and Function*. Academic Press, NY.
51. Rouzina, I. and Bloomfield, V.A. (1999) Heat capacity effects on the melting of DNA. I. General aspects. *Biophys. J.*, **77**, 3242–3251.
52. Zahn, R., Liu, A., Luhrs, T., Riek, R., von Schroetter, C., Lopez Garcia, F., Billeter, M., Calzolari, L., Wider, G. and Wuthrich, K. (2000) NMR solution structure of the human prion protein. *Proc. Natl Acad. Sci. USA*, **97**, 145–150.
53. Knaus, K.J., Morillas, M., Swietnicki, W., Malone, M., Surewicz, W.K. and Yee, V.C. (2001) Crystal structure of the human prion protein reveals a mechanism for oligomerization. *Nat. Struct. Biol.*, **8**, 770–774.
54. Ivanyi-Nagy, R., Davidovic, L., Khandjian, E.W. and Darlix, J.L. (2005) Disordered RNA chaperone proteins: from functions to disease. *Cell Mol. Life Sci.*, **62**, 1409–1417.
55. Tompa, P. and Csermely, P. (2004) The role of structural disorder in the function of RNA and protein chaperones. *FASEB J.*, **18**, 1169–1175.
56. Lysek, D.A., Schorn, C., Nivon, L.G., Esteve-Moya, V., Christen, B., Calzolari, L., von Schroetter, C., Fiorito, F., Herrmann, T., Guntert, P. et al. (2005) Prion protein NMR structures of cats, dogs, pigs, and sheep. *Proc. Natl Acad. Sci. USA*, **102**, 640–645.
57. Lopez Garcia, F., Zahn, R., Riek, R. and Wuthrich, K. (2000) NMR structure of the bovine prion protein. *Proc. Natl Acad. Sci. USA*, **97**, 8334–8339.
58. Zeng, Y., Liu, H.W., Landes, C.F., Kim, Y.J., Ma, X., Zhu, Y., Musier-Forsyth, K. and Barbara, P.F. (2007) Probing nucleation, reverse annealing, and chaperone function along the reaction path of HIV-1 single-strand transfer. *Proc. Natl Acad. Sci. USA*, **104**, 12651–12656.
59. Chen, Y., Balakrishnan, M., Roques, B.P. and Bambara, R.A. (2003) Steps of the acceptor invasion mechanism for HIV-1 minus strand strong stop transfer. *J. Biol. Chem.*, **278**, 38368–38375.
60. Kim, J.K., Palaniappan, C., Wu, W., Fay, P.J. and Bambara, R.A. (1997) Evidence for a unique mechanism of strand transfer from the transactivation response region of HIV-1. *J. Biol. Chem.*, **272**, 16769–16777.
61. Liu, H.W., Cosa, G., Landes, C.F., Zeng, Y., Kovaleski, B.J., Mullen, D.G., Barany, G., Musier-Forsyth, K. and Barbara, P.F. (2005) Single-molecule FRET studies of important intermediates in the nucleocapsid-protein-chaperoned minus-strand transfer step in HIV-1 reverse transcription. *Biophys. J.*, **89**, 3470–3479.
62. Cristofari, G., Ivanyi-Nagy, R., Gabus, C., Boulant, S., Lavergne, J.P., Penin, F. and Darlix, J.L. (2004) The hepatitis C virus Core protein is a potent nucleic acid chaperone that directs dimerization of the viral (+) strand RNA in vitro. *Nucleic Acids Res.*, **32**, 2623–2631.
63. Ivanyi-Nagy, R., Kanevsky, I., Gabus, C., Lavergne, J.P., Ficheux, D., Penin, F., Fosse, P. and Darlix, J.L. (2006) Analysis of hepatitis C virus RNA dimerization and core-RNA interactions. *Nucleic Acids Res.*, **34**, 2618–2633.
64. Vo, M.N., Barany, G., Rouzina, I. and Musier-Forsyth, K. (2009) HIV-1 nucleocapsid protein switches the pathway of transactivation response element RNA/DNA annealing from loop-loop “kissing” to “zipper”. *J. Mol. Biol.*, **386**, 789–801.
65. Godet, J. and Mely, Y. (2010) Biophysical studies of the nucleic acid chaperone properties of the HIV-1 nucleocapsid protein. *RNA Biol.*, **7**, 48–60.
66. Summers, M.F., Henderson, L.E., Chance, M.R., Bess, J.W. Jr, South, T.L., Blake, P.R., Sagi, I., Perez-Alvarado, G., Sowder, R.C. 3rd, Hare, D.R. et al. (1992) Nucleocapsid zinc fingers detected in retroviruses: EXAFS studies of intact viruses and the solution-state structure of the nucleocapsid protein from HIV-1. *Protein Sci.*, **1**, 563–574.
67. Morellet, N., de Rocquigny, H., Mely, Y., Jullian, N., Demene, H., Ottmann, M., Gerard, D., Darlix, J.L., Fournie-Zaluski, M.C. and Roques, B.P. (1994) Conformational behaviour of the active and inactive forms of the nucleocapsid NCp7 of HIV-1 studied by 1H NMR. *J. Mol. Biol.*, **235**, 287–301.
68. Muriaux, D. and Darlix, J.L. (2010) Properties and functions of the nucleocapsid protein in virus assembly. *RNA Biol.*, **7**, 744–753.
69. Darlix, J.L., Garrido, J.L., Morellet, N., Mely, Y. and de Rocquigny, H. (2007) Properties, functions, and drug targeting of the multifunctional nucleocapsid protein of the human immunodeficiency virus. *Adv. Pharmacol.*, **55**, 299–346.
70. Oberosler, P., Hloch, P., Ramsperger, U. and Stahl, H. (1993) p53-catalyzed annealing of complementary single-stranded nucleic acids. *EMBO J.*, **12**, 2389–2396.
71. Malaga-Trillo, E. and Sempou, E. (2009) PrPs: Proteins with a purpose: lessons from the zebrafish. *Prion*, **3**, 129–133.
72. Chakrabarti, O., Ashok, A. and Hegde, R.S. (2009) Prion protein biosynthesis and its emerging role in neurodegeneration. *Trends Biochem. Sci.*, **34**, 287–295.
73. Wickner, R.B., Edskes, H.K., Shewmaker, F.P., Kryndushkin, D., Nemecek, J., McGlinchey, R. and Bateman, D. (2010) The Relationship of Prions and Translation. *WIREs RNA*, **1**, 81–89.
74. Si, K., Lindquist, S. and Kandel, E.R. (2003) A neuronal isoform of the amyloid CPEB has prion-like properties. *Cell*, **115**, 879–891.
75. Gomes, M.P., Cordeiro, Y. and Silva, J.L. (2008) The peculiar interaction between mammalian prion protein and RNA. *Prion*, **2**, 64–66.
76. Gomes, M.P., Millen, T.A., Ferreira, P.S., e Silva, N.L., Vieira, T.C., Almeida, M.S., Silva, J.L. and Cordeiro, Y. (2008) Prion protein complexed to N2a cellular RNAs through its N-terminal domain forms aggregates and is toxic to murine neuroblastoma cells. *J. Biol. Chem.*, **283**, 19616–19625.
77. Cordeiro, Y., Machado, F., Juliano, L., Juliano, M.A., Brentani, R.R., Foguel, D. and Silva, J.L. (2001) DNA converts cellular prion protein into the beta-sheet conformation and inhibits prion peptide aggregation. *J. Biol. Chem.*, **276**, 49400–49409.
78. Deleault, N.R., Lucassen, R.W. and Supattapone, S. (2003) RNA molecules stimulate prion protein conversion. *Nature*, **425**, 717–720.
79. Silva, J.L., Lima, L.M., Foguel, D. and Cordeiro, Y. (2008) Intriguing nucleic-acid-binding features of mammalian prion protein. *Trends Biochem. Sci.*, **33**, 132–140.
80. Kocisko, D.A., Vaillant, A., Lee, K.S., Arnold, K.M., Bertholet, N., Race, R.E., Olsen, E.A., Juteau, J.M. and Caughey, B. (2006) Potent antiscrapie activities of degenerate phosphorothioate oligonucleotides. *Antimicrob. Agents Chemother.*, **50**, 1034–1044.